Available online at www.sciencedirect.com
ScienceDirect
Geochimica et Cosmochimica Acta 71 (2007) 1563–1573
Geochimica et Cosmochimica Acta
www.elsevier.com/locate/gca

# Oxygen self-diffusion "fast-paths" in titanite single crystals and a general method for deconvolving self-diffusion profiles with "tails"

X.Y. Zhang [a,b,*], E.B. Watson [a], D.J. Cherniak [a]

[a] Department of Earth and Environmental Sciences, Rensselaer Polytechnic Institute, Troy, NY 12180, USA
[b] Department of Geosciences, 1040 E. 4th Street, The University of Arizona, Tucson, AZ 85721, USA

Received 19 May 2006; accepted in revised form 7 December 2006; available online 24 December 2006

**Abstract**

Like most other minerals, titanite rarely if ever forms perfect crystals. In addition to the point defects that might affect lattice diffusion, there may be extended line- or planar defects along which fast diffusion could occur. During the course of an experimental study of oxygen lattice diffusion in titanite, we found that almost all of the $^{18}O$ uptake profiles produced in natural titanite crystals departed from the complementary error function solution expected for simple lattice diffusion with a constant surface concentration. Instead, they exhibited "tails" extending deeper into the samples than expected for simple lattice diffusion. The purpose of this contribution is to report on these features—described as "fast-paths" for oxygen diffusion—and outline a method for coping with them in extracting information from diffusion profiles.

For both dry and hydrothermal experiments in which the "fast paths" are observed, $^{18}O$ was used as the diffusant. In dry experiments, the source material was $^{18}O$-enriched $SiO_2$ powder, while $^{18}O$-enriched water was used for the hydrothermal experiments. Diffusive uptake profiles of $^{18}O$ were measured in all cases by nuclear reaction analysis (NRA) using the $^{18}O(p,\alpha)^{15}N$ reaction [see Zhang X. Y., Cherniak D. J., and Watson E. B. (2006) Oxygen diffusion in titanite: lattice and fast-path diffusion in single crystals. *Chem. Geol.* **235** 105–123].

In our experiments, different sizes of "tails" (with varying $^{18}O$ concentrations) were observed. Theoretically, under the same temperature and pressure conditions, the sizes of tails should be affected by two factors: the diffusion duration and the defect density. For the same experiment duration, the higher the defect density, the larger the "tail"; for the same defect densities, the longer the diffusion duration, the larger the "tail."

The diffusion "tails" could be a result of either planar defects or one-dimensional "pipe" diffusion. AFM imaging of HF etched titanite surfaces confirmed that the etched features might be caused by either parallel planar defects or parallel pipe defects, but could not differentiate between these possibilities. Through theoretical calculations simulating the tailed diffusion profiles using reasonable assumptions of lattice diffusivities and fast-path diffusivities, and comparing these with tail features measured in our samples, it can be concluded that the "tails" observed in our experiments are caused by planar defects rather than pipe defects.

A new method was developed for separating the "fast-path" contribution from the overall composite diffusion profile consisting of both "fast-path" and lattice diffusion. Through this process, the lattice diffusion coefficient could be determined, which is required to analyze the tail. The oxygen diffusion rates in the fast-paths were obtained by traditional graphical analysis methods, using the Whipple–Le Claire equation (for 2-D defects) assuming that the width of the fast-path is 1 nm. Two Arrhenius relations were obtained for the fast-path diffusion phenomenon, one for experiments under dry conditions, and the other for hydrothermal conditions:

$$D_{\mathrm{dry}} = 4.03 \times 10^{-2}(\mathrm{m^2/s})\exp(-313 \pm 22)\ (\mathrm{kJ/mol})/RT$$

$$D_{\mathrm{wet}} = 3.48 \times 10^{-7}(\mathrm{m^2/s})\exp(-219 \pm 39)\ (\mathrm{kJ/mol})/RT$$

* Corresponding author. Fax: +1 520 621 2672.
*E-mail address:* zhangxy@email.arizona.edu (X.Y. Zhang).

0016-7037/$ - see front matter 
doi:10.1016/j.gca.2006.12.013

Along with the lattice diffusivity, the presence and 3-D distribution of any fast-paths—and the diffusivities in these paths—are important to the bulk closure properties of single crystals. For titanites, AFM imaging showed that the fast-paths may not be interconnected at a length-scale comparable with the crystal dimension, so they may not have a significant effect on bulk closure properties.


## 1. INTRODUCTION

Natural crystals are far from ideal crystals. Consequently, even when high-quality crystals free of apparent cracks and inclusions are chosen for lattice diffusion studies, contributions from "fast-paths" may be observed in the form of diffusion profiles exhibiting "tails" (Reddy and Cooper, 1982; Yurimoto et al., 1989; Cawley et al., 1991; Prot and Monty, 1996; Watson and Cherniak, 1997; Moore et al., 1998; Amami et al., 1999). These "tailed" diffusion profiles are evidence that there exists another diffusion pathway besides the crystal lattice. Earlier studies did not attempt to understand observed tails in detail, because these were limited in extent and present in only a small fraction of all the experiments. In such cases, ignoring the small tails will not appreciably affect interpretation of the measurements in terms of lattice diffusion. In some diffusion studies it has been found that for single crystals of certain minerals (e.g., rutile, forsterite, $\alpha$-$Al_2O_3$, $\alpha$-$Fe_2O_3$, titanite), almost all the diffusion profiles are "tailed", and tail sizes vary widely (Yurimoto et al., 1992; Prot and Monty, 1996; Moore et al., 1998; Amami et al., 1999; Zhang et al., 2006). In order to obtain meaningful results and extract lattice diffusivities from these concentration profiles, the physical nature of these diffusion "fast-paths" needs to be understood in order to tailor the mathematical model used to fit the profiles. It is also essential in applying the diffusion data to geological systems to assess whether "fast-paths" affect the bulk closure properties of minerals.

Despite their frequent observation, there is no established protocol for dealing with "tailed" diffusion profiles. In previous studies, two methods have been used to fit these types of profiles. Behind the two methods are different assumptions regarding the nature of fast-paths. One method involves fitting tailed diffusion profiles with two separate error functions, as done by Moore et al. (1998) in their study of oxygen diffusion in rutile. Their assumption is that two different lattice diffusion mechanisms—one slow, the other fast—are responsible for the overall profiles. If this assumption were accurate, the slow diffusion path would not be observed at all unless the two mechanisms were completely independent of one another. Therefore, this treatment of the diffusion profiles may not be appropriate. The case of rutile is also complicated by its potential for large deviations from stoichiometry. The other approach treating tailed diffusion profiles is based on the observation that the tails themselves strongly resemble diffusion profiles resulting from grain-boundary diffusion in polycrystalline materials. This treatment was presented by Yurimoto and Nagasawa (1989) and Yurimoto et al. (1992). Because they used a mathematical model for polycrystalline materials with grain boundaries to fit their data, they made the assumption that the fast-paths are like grain boundaries, even though this assumption was not explicitly stated in their papers. Several similar treatments later appeared, for example for oxygen diffusion in corundum (Prot and Monty, 1996), and oxygen diffusion in hematite (Amami et al., 1999). However, the authors did not discuss in detail their assumptions and reasons for selecting these models. Efforts were made to characterize the fast diffusion paths in the case of oxygen diffusion in corundum (e.g., Le Gall and Lesage, 1994), where TEM imaging revealed parallel planar defect features. Because of the mismatch in scales of the features themselves (conceivably as small as nanometers) and the area to be searched (millimeters in some cases), direct observation of the fast diffusion paths is generally very difficult.

The need for the present study became evident when we measured oxygen lattice diffusion using natural gem quality titanite (Zhang et al., 2006). Instead of observing diffusion profiles that were complementary error function curves—which would conform to our boundary conditions of diffusion into a semi-infinite medium with constant surface concentration—almost all the acquired diffusion profiles showed tails, with sizes varying from very small to quite substantial relative to the inferred lattice diffusion profile (see examples in Fig. 1). This provided us an excellent opportunity to explore the proper method to fit these complicated diffusion profiles, which would involve understanding the essence of the fast-paths and choosing the proper mathematical solution. Our assumption is that the fast-paths are physical defects in the crystals. These defects might be line defects or planar defects at the nano-scale, or a combination of both. We modeled the two possibilities and concluded that planar defects are the likely fast-paths for oxygen diffusion in titanite. Line defects might exist as well, but they cannot make measurable contributions to the diffusion profiles observed by the techniques available.

The aforementioned defects might be more common than previously thought. The details of the specific techniques used to characterize diffusion profiles must be examined in order to understand why effects on diffusion of these kinds of defects might be observed under some circumstances and not others.

Because oxygen diffusion in crystals is generally slow (typically $10^{-15}$ to $10^{-22}$ $m^2/s$ over the range $\sim$750 to $\sim$1300 °C), the length scales of laboratory-generated diffusion profiles are usually sub-micron. At this scale, the profiling methods generally used are Nuclear Reaction Analysis (NRA) or Secondary Ion Mass Spectrometry (SIMS) depth profiling. In both methods, the analyses integrate over a large sample surface area relative to the diffusion depth. In other words, the volume measured by the profiling method is a thin-skin circle or square from which

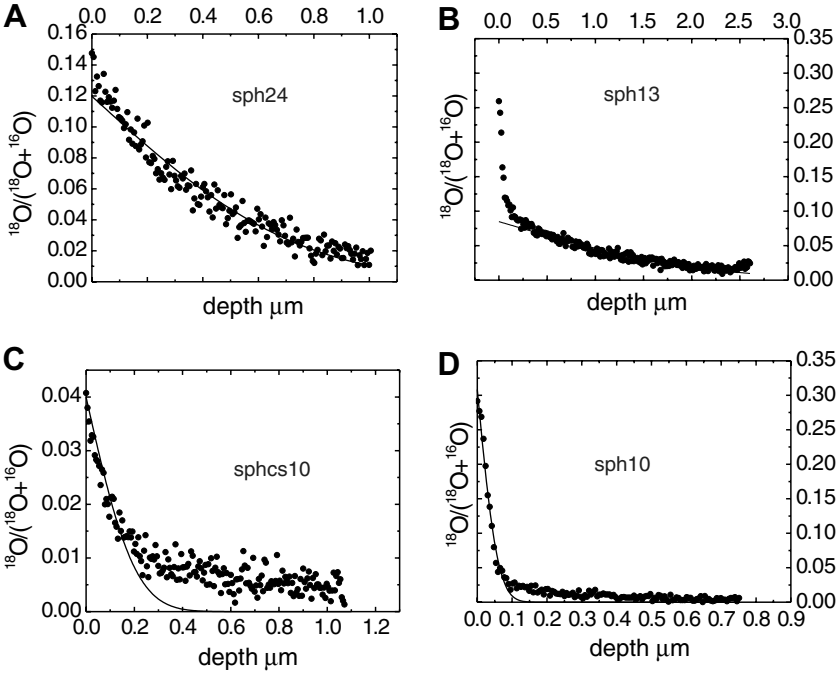


Fig. 1. Composite diffusion profiles showing evidence of more than one diffusion mechanism. (A) The profile departs from a simple error function fit, but this departure is difficult to recognize until an attempt is made to fit to a simple error function solution. There is no obvious break in slope which can distinguish the "tail"of the profile from the near-surface portion. (B) Large "tail" (C) intermediate "tail" (D) small "tail". Curves are error function fits that capture the most prominent feature of each profile. (B–D) have an obvious 'break point' that separates the "tail" from the near-surface steep part of the profile.

an average depth profile over a relatively large area is obtained. If line- and/or planar defects are present, each measurement could encompass many of them, depending on the defect combination and density. Because both the radii of pipes and the thicknesses of planar defects are on the scale of nanometers (Joesten, 1991), their contribution to measured diffusion profiles will not be significant unless these defects reach a certain density. In most cases some line- and/or planar defects are likely to be present, but if they do not reach a significant concentration, standard profiling methods cannot detect them, and only lattice diffusion will be observed. In such cases, lattice diffusion generally would control overall transport because of the much greater number of atoms present in the lattice relative to the defects. Only when the fast-paths reach a certain concentration in the crystal will they contribute an extended "tail" to the measured diffusion profile, causing a departure of this profile from that expected for lattice diffusion.

Comparison of atomic force microscopy (AFM) images obtained on HF vapor-etched natural titanite and synthetic titanite indicated that the fast-paths are either planar defects or pipe defects (Fig. 2). Below we will discuss these two possible models and show why the pipe model fails to describe the observed fast-path behavior. We will also explain the rationale for modifying the existing method of fitting the composite diffusion profiles to the planar model, and estimate the uncertainty in this fitting method using an example profile. Finally, the effect of these fast-paths on the bulk crystal closure properties is discussed.

## 2. MATERIALS AND METHODS

As discussed in the introduction, the oxygen diffusion experiments on titanite were not designed to measure fast-path diffusion specifically, but rather oxygen lattice diffusion in single crystals. Great care was taken to choose gem quality crystal pieces to avoid any complexities in the diffusion profiles that might be caused by imperfect crystals. The pieces were cut into 1-mm thick wafers, polished using a series of alumina powders down to 0.3 μm, then cut into 1.5-mm squares. After polishing, the slabs were screened carefully under a microscope to exclude these pieces with visible inclusions and micro-cracks. The selected slabs were pre-annealed at elevated temperature under controlled oxygen fugacity (to buffer at QFM) comparable to the experimental conditions. These slabs were run either at dry QFM-buffered conditions or wet at NNO-buffered conditions surrounded by $^{18}O$-enriched sources of diffusant (see Zhang et al., 2006 for detailed configurations of diffusion experiment capsules and experimental run conditions). The boundary condition for these diffusion experiments was a semi-infinite medium with a constant surface concentration. The diffusion profiles should conform to a complementary error function solution if lattice diffusion alone occurs during the experimental annealing. A multitude of previous studies at RPI and in other laboratories confirm this expectation.

The run products were recovered and cleaned using distilled water and ethanol in an ultrasonic bath, and then dried in a drying oven. The crystal slabs were usually broken into several pieces during the hydrothermal

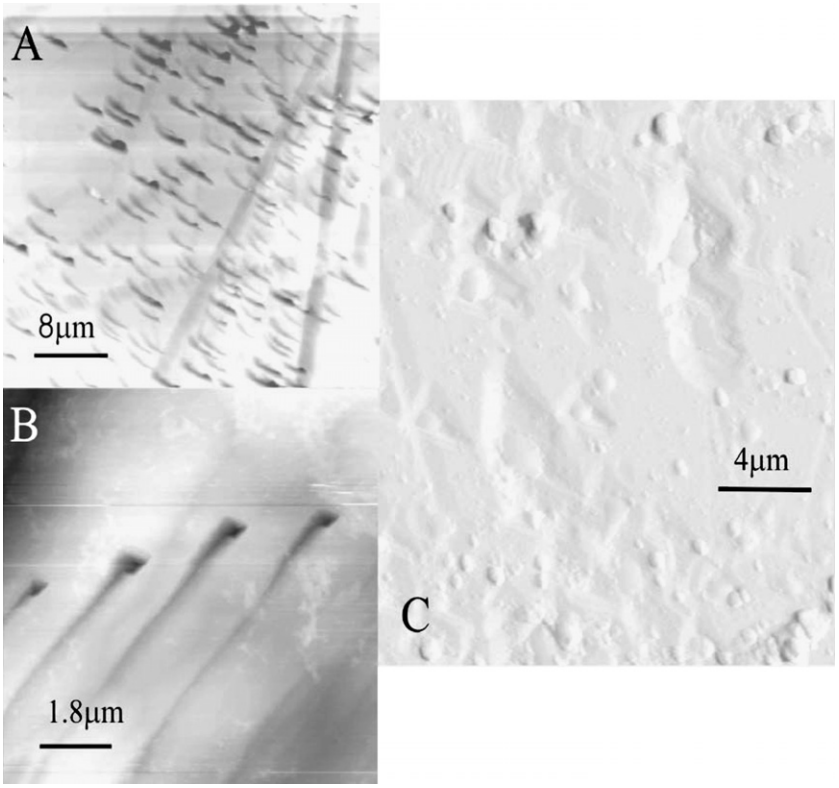


Fig. 2. AFM images of HF etched titanite surfaces. (A) and (B) are images of etched grooves on natural titanite surfaces. (C) Is an image of triangle-shaped etch pits on a synthetic titanite surface.

experiments, but in most cases a relatively large fragment with a polished surface could be recovered. These fragments were mounted in a small epoxy mount with the polished surface exposed for analysis.

The samples were analyzed by NRA to obtain the oxygen diffusion profiles (concentration of $^{18}O$ *vs.* depth). For the slabs, a ~1-mm$^2$ beam size was used; for the smaller fragments mounted in epoxy, a slightly smaller beam size, achieved by restricting the beam with slits, was used (see Cherniak, 1990 for a discussion of the principles of NRA and extraction of oxygen concentration profiles). The general length range of our measured diffusion profiles was 0.2–1.5 μm.

Almost all measured oxygen diffusion profiles from three different natural titanite crystals departed from the simple complementary error function solution, showing tails extending to much greater depth than the expected lattice-diffusion length-scale (see Fig. 1). In order to create a 'benchmark' against which to evaluate the composite (tailed) profiles and obtain robust lattice diffusivities, we synthesized ~1-mm size "perfect" titanite crystals (details of the synthesis method will be published separately). These synthetic titanites yielded $^{18}O$ diffusion profiles that conform very well to a simple complementary error function solution, suggesting that only lattice diffusion occurs in the synthetic crystals. The resulting diffusivities are important as constraints in fitting the composite profiles, and confirm the validity of our model and fitting method (see Zhang et al., 2006 for details).

## 3. OBSERVATIONS AND MODEL FOR FITTING PROFILES

The two segments of the diffusion profiles consist of a near-surface steep segment and an extended less-steep segment referred to as a "tail" (Fig. 1B–D). As previously noted, the tails were observed to vary from very small to relatively large in size (see Fig. 1). It is sometimes difficult to observe the deviation from a simple complementary error function profile until an attempt is made to fit the profile and extract a diffusivity (Fig. 1A and D). The composite nature of many profiles then becomes readily apparent, and raises the possibility of obtaining diffusion data for both the lattice and fast-path, on the operating assumption that the fast-paths consist of planar defects.

### 3.1. What are the fast-paths in single-crystal titanite?

No imperfections are evident in either the natural or the synthetic titanite crystals under optical microscopy, but it is clear that these crystals differ in some way because they show different diffusion behavior. The presence of extended defects in the natural titanites is implied. The general shapes of the $^{18}O$ diffusion profiles are not inconsistent with the presence of sub-grain boundaries dividing the grain into "domains" and making the overall character comparable to that of a polycrystalline material. Without further constraints, however, the defects could also be pipe-like in nature, and might or might not be inter-connected.

To further explore the character of the defects, we etched both natural and synthetic titanite slabs by exposing them to concentrated HF vapor for 30 s (the slabs had been polished and pre-annealed in the same manner as those used for the diffusion experiments). Atomic force microscopy (AFM) of the titanite surfaces revealed two features: triangle-shaped etched pits and elongated etched grooves (Fig. 2). The grooves were seen only on surfaces of the natural titanite crystals, localized within restricted areas and parallel to one another. The etched surfaces of synthetic titanites show only triangular etched pits. Based on their geometry, these appear to be controlled by the manner in which HF attacks the titanite lattice, while the grooves may represent etched versions of extended defects. Planar defects cannot be distinguished from one-dimensional (pipe) defects, but the atomic force microscopy does suggest that these extended defects are parallel to one another and not interconnected at a scale remotely approaching the crystal size.

### 3.2. Planar defects vs. pipes

There are two types of defects that are considered as possible contributors to the observed "tails" in the oxygen diffusion profiles. One of these is a linear dislocation of the lattice; these one-dimensional defects are very common in natural crystals, and often referred to as dislocation pipes. The other is linear dislocations, and parallel defects that form planar "dislocation walls"; these are two-dimensional features. These terms are conceptual when used to discuss the defects revealed by diffusion experiments. It is likely that pipe defects are more common than planar defects, and that these defects are probably neither evenly distributed nor parallel.

Models have been developed that can be used to describe diffusion in a medium containing these types of defects. In obtaining analytical solutions, many assumptions have been made to make the problems more tractable. Both of the models have been derived from models considering a single pipe or plane, and assume that pipes or planar defects are parallel and evenly distributed in order to model the overall effects of defects on bulk diffusion profiles. The models and resulting equations describing diffusion are outlined below.

#### *3.2.1. Planar model*

A model incorporating planar features of high diffusivity is commonly used to extract information from diffusion profiles in polycrystalline materials (Le Claire, 1963) in which case the planar features are grain boundaries. This model is also suitable for single crystals containing fast diffusion paths ('defects') of planar geometry. For simplicity, the model assumes that the planar defects are evenly distributed through the bulk diffusion medium (in the present case a single crystal), normal to the surface on which the diffusant is introduced, and of uniform thickness (see Fig. 3). With this configuration, the diffusant enters the crystal from the planar surface source by direct lattice diffusion, and also along the parallel planar defects. Because diffusion through the planar defects is faster, deeper penetration into the crystal occurs along the defects and locally into the adjacent lattice, resulting in what might be thought of as a "leakage field" in the vicinity of the defect.

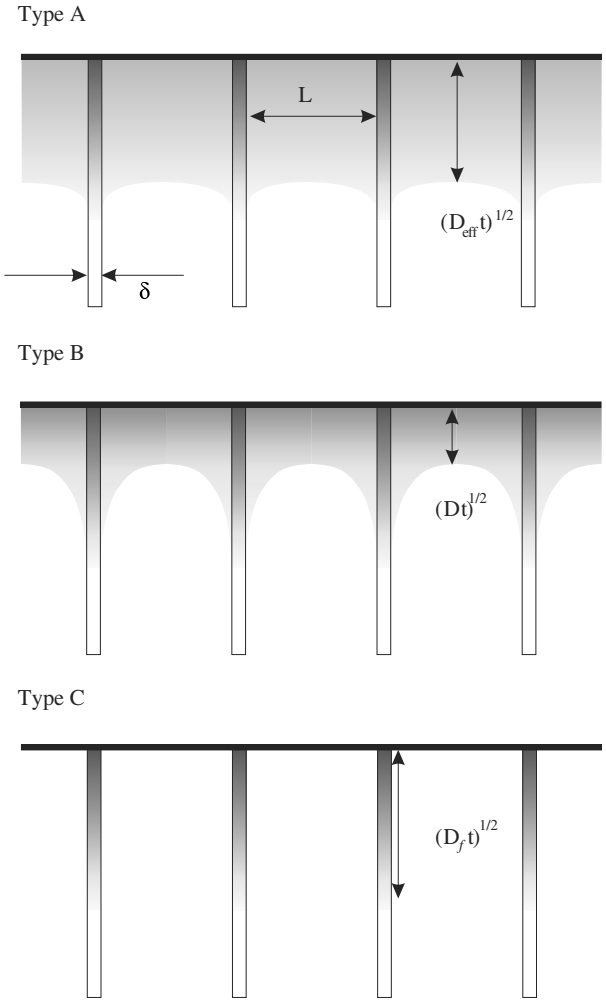


Fig. 3. Schematic illustration of types A, B and C diffusion kinetics in a single crystal material containing uniformly spaced planar fast diffusion paths. Modified from Mishin and Herzig (1999); see text for details.

Using the relative magnitudes of the "leakage fields" and the lattice diffusion field directly from the crystal surface, Harrison (1961) proposed a classification of three types of diffusion kinetics. Fig. 3 shows a schematic illustration of types A, B and C diffusion kinetics. (1) *Type A* refers to the case of long diffusion anneal times, small spacing between fast-paths, and/or a lattice diffusion coefficient not much smaller than the fast-path diffusion coefficient, so that the lattice diffusion length is much larger than the spacing between the fast-paths, and the "leakage fields" from different fast-paths overlap each other extensively. The concentration profile of the whole system (lattice plus defects) obeys Fick's law with $D_{\text{eff}} = fD_{\text{f}} + (1\text{-}f)D$, where $D$ and $D_{\text{f}}$ are the diffusivities in lattice and fast-paths, respectively, $D_{\text{eff}}$ is the effective bulk diffusivity, and $f$ is the volume fraction of fast-paths in the bulk material. (2) In *Type B* kinetics the same general phenomena occur, but the fast-path

spacing is large enough for them to be considered as isolated. The diffusion profiles in the Type B domain consist of two distinct parts: a steep, high-concentration part close to the source, which is mainly characteristic of lattice diffusion, and a low concentration flat part (“tail”) in the deeper region that represents fast-path diffusion. (3) *Type C* kinetics pertains to the case of short diffusion annealing times and/or lattice diffusion coefficients ($D$) negligibly small compared to the fast-path diffusion coefficients ($D_f$). Under these conditions, diffusion may be considered as taking place solely within the fast-paths.

For the above three circumstances, it is only in the case of Type B kinetics that an analytical solution can be applied to the bulk diffusion profiles in order to characterize both $D$ and $D_f \times \delta$, where $\delta$ is the thickness of the planar defects. In Type B kinetics, the fast-paths are considered to be isolated; as in polycrystalline materials, they are also appropriately modeled as parallel to one another, as demonstrated by Levine and MacCallum (1960).

In our complex diffusion profiles, we find that most of the profiles are Type B, but we also observed Type A profiles and an intermediate type between the two. For details see Zhang et al. (2006).

To obtain the averaged diffusion profile solution for the planar model with Type B kinetics, the diffusion profile for a solid with a single fast-path (Whipple, 1954) is integrated, and the solution was determined by Kaur and Gust (1989) as following:

$$\overline{C}(\eta,\beta) = C_0\mathrm{erfc}(\eta/2) + \frac{C_0(Dt)^{1/2}}{L}\frac{2\eta}{\pi^{1/2}} \times \int_1^{\Delta} \frac{\exp(-\eta^2/4\sigma)}{\sigma^{3/2}}\left(\frac{\Delta-\sigma}{\Delta-1}\right)^{1/2} \times \left[\frac{\exp(-Y^2)}{\pi^{1/2}} - Y\mathrm{erfc}(Y)\right]\mathrm{d}\sigma \quad (1)$$

where $Y = \frac{\sigma-1}{2\beta}\left(\frac{\Delta-1}{\Delta-\sigma}\right)^{1/2}$ and $\varepsilon$, $\eta$, $\beta$ and $\Delta$ are dimensionless variables corresponding to $y$, $z$, $t$ and $D_f/D$, defined as follows by Whipple in order to make the diffusion equation solvable:

$$\varepsilon = \frac{y-\delta/2}{(Dt)^{1/2}}$$
$$\eta = \frac{z}{(Dt)^{1/2}}$$
$$\beta = \frac{(\Delta-1)\delta}{2(Dt)^{1/2}} \approx \frac{\delta D_f}{2D^{3/2}t^{1/2}}$$
$$\Delta = \frac{D_f}{D}$$

In these variables, $y$ is the direction perpendicular to the fast-path, $z$ is the direction parallel to the fast-path, $t$ is the diffusion time, $D$ is the lattice diffusivity and $D_f$ is the fast-path diffusivity.

Included but not obvious in Eq. (1) is the presence of a defect density term. The diffusion fields from adjacent defects separated by distance $L$ will begin to overlap when $4(Dt)^{1/2} > L$. It is reasonable to define a defect density factor which ranges from 0 to 1, as $F = 4(Dt)^{1/2}/L$. This is a relative defect density factor which is time-dependent. With this definition, the above equation becomes:

$$\overline{C}(\eta,\beta) = C_0\mathrm{erfc}(\eta/2) + FC_0\frac{\eta}{2\pi^{1/2}} \times \int_1^{\Delta} \frac{\exp(-\eta^2/4\sigma)}{\sigma^{3/2}}\left(\frac{\Delta-\sigma}{\Delta-1}\right)^{1/2} \times \left[\frac{\exp(-Y^2)}{\pi^{1/2}} - Y\mathrm{erfc}(Y)\right]\mathrm{d}\sigma \quad (2)$$

The first term of this equation, $C_0\mathrm{erfc}(\eta/2)$, is the contribution to the average profile from diffusion directly from the surface into bulk through lattice diffusion; the second term is the contribution to the average profile from the diffusant carried by the fast-paths, which then enters the normal lattice through lattice diffusion.

### 3.2.2. Pipe model

The above diffusion kinetics classification is also valid for parallel pipe diffusion, and for the same reasons the governing diffusion equation is solvable only in the Type B regime. Le Claire and Rabinovitch (1981) derived an exact solution for a constant surface source for an average diffusion profile for a relatively large measured area:

$$\overline{C} = C_0\mathrm{erfc}(\eta/2) + C_0\varepsilon_d^2\frac{16\beta_d^2}{\pi^3\alpha_d^2}\int_0^{\infty} x^3\exp(-x^2)\sin(\eta x)\mathrm{d}x \times \int_0^{\infty}\frac{[1-\exp(-y^2)]}{(\theta_d^2+\phi_d^2)}\mathrm{d}y \quad (3)$$

where $\eta = \frac{z}{(Dt)^{1/2}}$; $\varepsilon_d^2 = \pi r_d^2\rho_d$; $\alpha_d = r_d/(Dt)^{1/2}$; $\beta_d = (\Delta_d - 1)\alpha_d$ and $\Delta_d = D_d/D$. Here $r_d$ is the dislocation pipe radius; $D$ and $D_d$ are the lattice diffusivity and diffusivity in the pipe, respectively, $\rho_d$ is the dislocation pipe density per area, $t$ is the diffusion annealing time and $z$ is the distance from the surface into the crystal along the pipe direction. In Eq. (3),

$$\theta_d = 2yY_1(y\alpha_d) + (x^2\beta_d - y^2\alpha_d)Y_0(y\alpha_d) \text{ and}$$
$$\phi_d = 2yJ_1(y\alpha_d) + (x^2\beta_d - y^2\alpha_d)J_0(y\alpha_d)$$

where $Y_0(x)$ and $Y_1(x)$ are the 0th and 1st order Bessel functions of the second kind, respectively, and $J_0(x)$ and $J_1(x)$ are the 0th and 1st order Bessel functions of the first kind.

### 3.2.3. Why the planar defect model is preferred in fitting these profiles

Because the AFM imaging is not definitive in identifying the fast-paths as planar defects or pipes, we calculated diffusion profiles using both models and compared the shape of these profiles with the experimentally observed profiles. We found that the planar defect model profiles look similar to the diffusion profiles we observed in this study—a steep profile in the near-surface region with a deeper flat tail, with an obvious break in slope between these two parts. Pipe diffusion profiles do not show an obvious separation point, and they have much shorter tails than planar-defect profiles if we assume the diffusivity is the same in the planar defects and pipes. The length of the tail is determined by lattice diffusivity, fast-path diffusivity, and the annealing time, while the magnitude of the tail is determined by the surface concentration and the defect density. The differences between the tails produced by diffusion along fast-transport pathways in planar and pipe models are largely a conse-

quence of the differences in dimensionality of the defects. Planar defects, as two-dimensional features, are analogous to grain boundaries in that there is greater opportunity for exchange within the defect given the spacing of dislocations; in contrast, pipe defects, as essentially one-dimensional features surrounded by nearly perfect crystal, provide less opportunity for long-distance diffusion within the defect without diffusion out into the normal lattice.

By fitting our diffusion profiles to the planar model, we determined that the diffusivities in planar fast-paths are 4–5 orders of magnitude greater than in the lattice, which is comparable with the difference between lattice diffusivities and grain-boundary diffusivities found in previous studies of various minerals (Farver and Yund, 1991, 1995; Prot et al., 1996; Farver and Yund, 1998). In order to form tails of length comparable to those observed using fast-path pipes, the pipe diffusivities would have to be much higher (by a few orders of magnitude) than the diffusivities we obtained by the planar defect model, which seems unlikely. Pipe defects might in fact coexist with planar defects, but in this case the pipes would not greatly affect the overall diffusion profiles. Fig. 4 shows a comparison of calculated diffusion profiles from the planar model and pipe model, both with the largest relative defect density (1). The pipe model shows a much shorter tail than the planar model. Fitting the pipe model profile with an error function results in a relatively poor fit, but the resulting lattice diffusivity is the same within error as that returned by fitting a planar model. Consequently, negligible error is introduced by ignoring any pipe defects that might be present.

### 3.3. Data fitting method

In principle, we should fit our tailed diffusion profiles to Eq. (1) to obtain diffusivities, but because the mathematics is so complex, such an approach is rarely used. Fortunately, through analysis of the function and exploring different $n$ values by plotting $\frac{\partial \ln \overline{C}}{\partial(\eta\beta^{-1/2})^n}$ *vs.* $\eta\,\beta^{-1/2}$, Le Claire (1963) found that at depths in the sample where direct lattice diffusion from the surface can be ignored (where the diffusion profile is the relatively flat tail segment), when $n = 6/5$, $\frac{\partial \ln \overline{C}}{\partial(\eta\beta^{-1/2})^n}$ *vs.* $\eta\beta^{-1/2}$ is very close to a horizontal straight line, with a value close to 0.78 for $\beta \geqslant 1$. This observation can be expressed as the following equation:

$$-\frac{\partial \ln \overline{C}}{\partial(\eta\beta^{-1/2})^{6/5}} \approx 0.78 \tag{4}$$

Based on this equation, he worked out the following relation which could be used to analyze the diffusion tail, now referred to as the Whipple–Le Claire equation:

$$\delta D_f \approx 1.332\sqrt{\frac{D}{t}}\left[\frac{\partial \ln \overline{C}}{\partial z^{6/5}}\right]^{-\frac{5}{3}} \tag{5}$$

where $\delta$ is the effective boundary thickness, $t$ is the annealing time, $z$ is the depth, and $\overline{C}$ is the average concentration in a slice perpendicular to the fast diffusion path.

With this information, the Whipple–Le Claire equation can be implemented graphically to fit the tail portion of a diffusion profile.

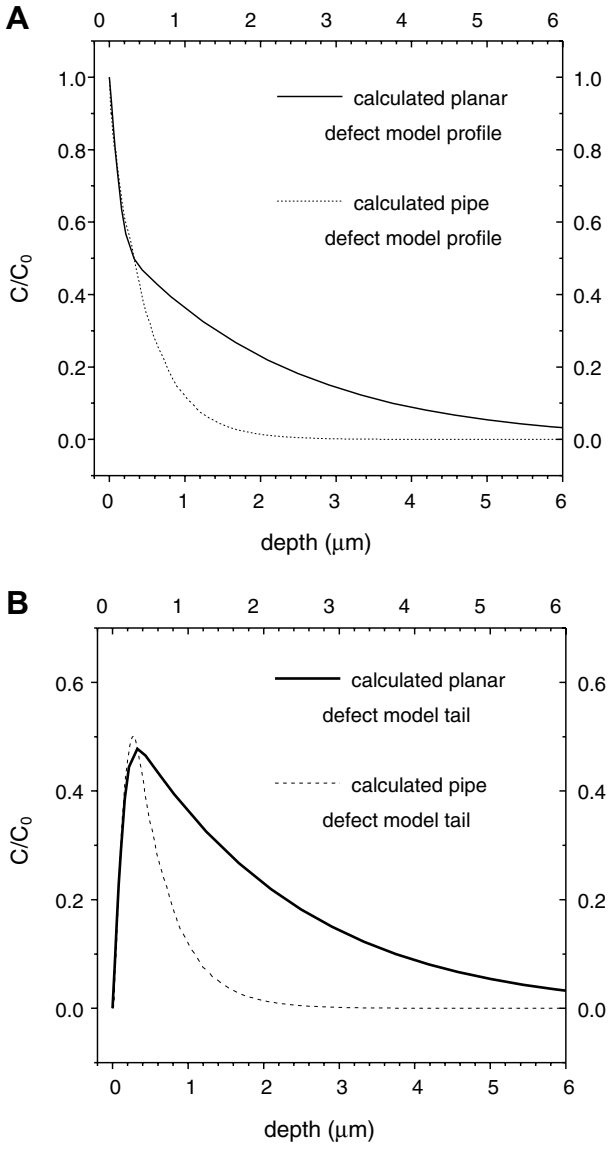


Fig. 4. (A) Comparison of profiles for a planar defect model and a pipe diffusion model with the same lattice diffusivity and fast-path diffusivity and the highest permitted defect density (relative defect density = 1). The parameters used for the planar defect model are: $D = 10^{-20}\,m^2/s$; $D_f = 10^{-15}\,m^2/s$; $\delta = 1$ nm; $t = 10^6$ s and $L = 10^{-7}$m; for the pipe model they are: $D = 10^{-20}\,m^2/s$; $D_d = 10^{-15}\,m^2/s$; $r_d = 1$ nm; $t = 10^6$ s and calculated $r_d = 6.6 \times 10^{13}/m^2$. (B) Comparison of the planar defect model "tail" with the pipe diffusion model "tail". The pipe diffusion model profile and "tail" are modified from Le Claire and Rabinovitch's (1981) numerically computed results.

#### *3.3.1. Existing method*

In applying the Whipple–Le Claire equation, the lattice diffusivity is needed in order to obtain the fast-path diffusivity. In order to analyze diffusion profiles on polycrystalline materials, the lattice diffusivity is usually measured in a separate experiment on a single crystal of the same material, but by using a single-crystal/polycrystal diffusion couple, it is possible to extract both lattice diffusion data and

grain-boundary diffusion data from a single experiment (Van Orman et al., 2003). In the case of crystals with extended defects, the lattice diffusivity is determined by the near-surface steep part of the diffusion profile (Prot and Monty, 1996; Amami et al., 1999; Zhang et al., 2006).

In some previous studies, attempts to fit "tailed profiles" were implemented in two steps. The lattice diffusivity was first obtained by fitting the near-surface steep segment directly to an error function solution. This lattice diffusivity was in turn used in the Whipple–Le Claire equation to obtain the fast-path diffusivity from the tail (Prot and Monty, 1996; Amami et al., 1999). This method ignores the contribution to the near-surface portion of the profile from fast diffusion paths, thus yielding larger apparent lattice diffusivities. As a consequence, the accuracy of the fast-path diffusivities was also compromised because this depends on the lattice diffusivity.

### 3.3.2. Modification

Our fitting method is implemented by two similar steps but with important modifications. Instead of fitting the near-surface steep segment directly as the lattice diffusion profile, as done in the studies cited above, we instead subtract the fast-path contribution from this part, recognizing that it contains contributions from both diffusion pathways. The second step is the same, in which the tail is analyzed using the Whipple–Le Claire equation. Because we obtain more accurate lattice diffusivities, we will obtain more accurate fast-path diffusivities as well.

Fig. 5 shows an example of a calculation of a diffusion profile evolving through time in a single crystal with planar defects. (A) Shows the overall diffusion profile. (B) Shows the contribution to the overall diffusion profile from the lattice diffusion from the surface and (C) shows the contribution due to fast-paths.

Based on the above observation, we implemented a simple modification: on the concentration *vs.* depth plot, we use a straight line segment from the origin (concentration 0 at depth 0) to the peak of the fast-path contribution curve to estimate the effect of the fast-path on the steep near-surface diffusion profile section. After subtracting this straight line segment from the near-surface part of the diffusion profile, the curve is then fit to the complementary error function solution to obtain the lattice diffusivity. Although this approach is an approximation, it yields a more accurate lattice diffusivity than the previous fitting method.

It should be noted that when the tail is small, these two methods give similar results, but when the tail is relatively large, the present method is significantly more accurate.

### 3.3.3. Fitting error estimation: an example

Because the method used to fit diffusion data is a graphical method, there are two possible approximations: (1) use a straight line segment to approximate the fast-path contribution to the near-surface portion of the composite diffusion profile. (2) Use the Whipple–Le Claire equation as a graphical estimate based on the observation that $\ln C$ *vs.* $z^{6/5}$ is close to a straight line. Either way, it is difficult to estimate the error of the fit in an analytical way.

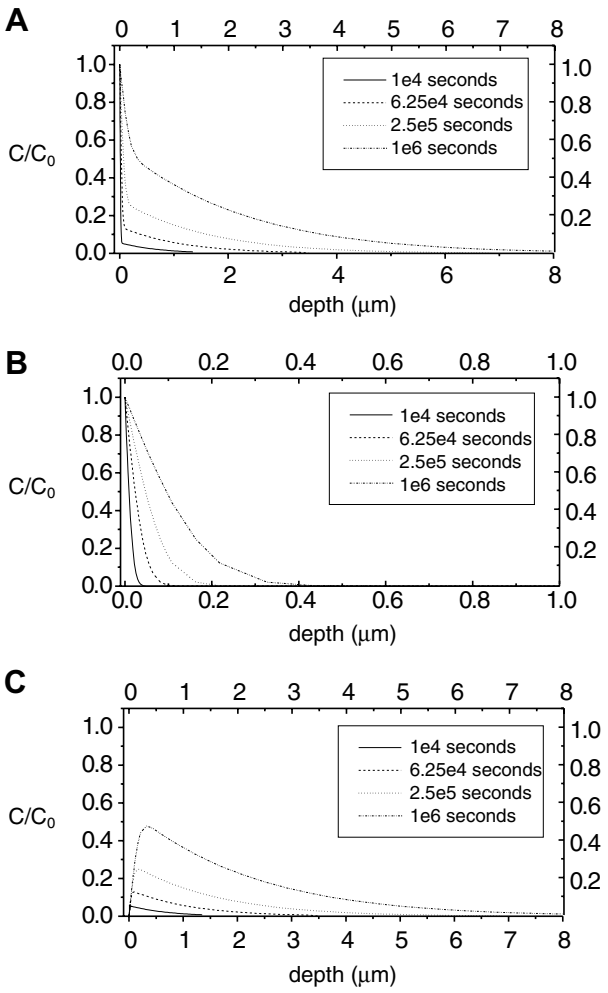


Fig. 5. An example calculation of the evolution through time of a Type B kinetics diffusion profile, with the following parameters: spacing $L = 4 \times 10^{-7}$ m, lattice diffusivity $D = 10^{-20}$ m$^2$/s, fast-path diffusivity $D_f = 10^{-15}$ m$^2$/s, fast-path thickness $\delta = 1$ nm. The boundary condition is constant surface concentration. (A) The evolution of the overall diffusion profile through time; $t = 10^6$ s is the upper time limit beyond which the diffusion profile will be moved to Type A regime, and $t = 10^4$ s is the lower time limit below which the tail is so small that ignoring it will not introduce significant error to the fitted lattice diffusivity. (B) Time evolution of the lattice diffusion contribution to the overall diffusion profile. (C) Time evolution of the fast-path contribution to the overall diffusion profile.

Here we calculate a composite profile and back fit the profile to obtain the diffusion parameters, and then compare the fitted diffusivities with the diffusivity we used in the model to get a sense of the range of the fitting errors.

The parameters used to calculate the composite profile are $D = 10^{-20}$ m$^2$/s, $D_f = 10^{-15}$ m$^2$/s, $t = 10^6$ s, $\delta = 1$ nm, and $F = 1$. (This last value is used because fitting of the tail is based on the slope of the $\ln C$ *vs.* $z^{6/5}$ line, and from the solution it is clear that $F$ affects the intercept but not the slope on the $\ln C$ *vs.* $z^{6/5}$ plot.) The fitting result is shown in Fig. 6. The fitted $D = (1.68 \pm 0.06) \times 10^{-20}$ m$^2$/s and fitted $D_f = 0.98 \times 10^{-15}$ m$^2$/s. It can be estimated that the fitting uncertainty is within a factor of 2, which is comparable to experimental uncertainty.

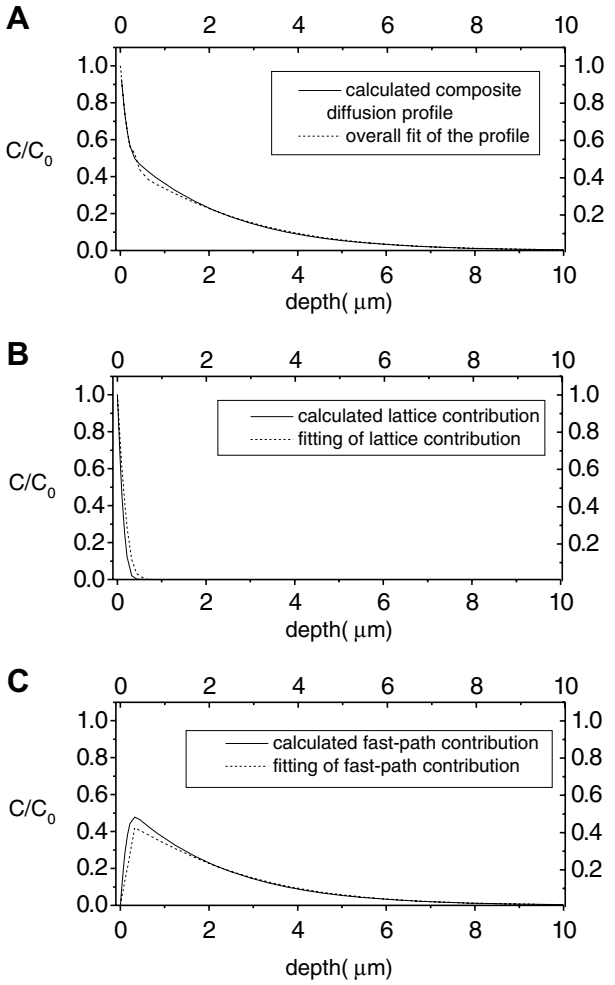


Fig. 6. An example of fitting of a calculated composite diffusion profile. (A) Overall fitting. (C) Fitting of the part of the profile due to fast-path diffusion. The solid curve is the calculated fast-path diffusion contribution to the overall diffusion profile, and the dashed curve is the fit to this part. (B) Calculated lattice diffusion contribution and the fitting to this part after subtracting the fast-path related contribution. See text for discussion.

## 4. DISCUSSION AND IMPLICATIONS

The mathematical solutions discussed above are suitable for describing self-diffusion. If the diffusants are trace elements, the partitioning of the element of interest between the bulk crystal lattice and the fast-paths has to be considered. By replacing $\delta D_f$ with $s\delta D_f$ in Eq. (5)—where $s$ is the partition coefficient of the element between the defect plane and normal lattice—the equation can still be used to analyze the tail part of the diffusion profile.

### 4.1. Observation window for Type B tails and the effects of relative defect density

Through Eq. (2) and Fig. 5, we can see that even if there are planar defects, we do not obtain a Type B "tailed" diffusion profile all the time. There is a window, depending on the relative defect density, over which the tail can be detected and analyzed using Eq. (5). The window is $F > 0.05$ to $F = 1$. For $F > 1$, the lateral diffusion fields of the adjacent defects overlap. For $F < 0.05$, the tail is below the detection limit. From the definition $F = 4(Dt)^{1/2}/L$, it can be noted that the relative defect density is a time-dependent variable, since $D$ and $L$ are definite values for certain sample at a certain temperature, so the $F$ window determines a time window within which the "tailed" diffusion profiles can be observed. This information is very useful to plan experimental durations if $L$ and $D$ are known. Unfortunately, in the case of fast-paths in single crystals, the above information generally is not known. Moreover, even slabs cut from the same crystal may have very different spacing parameters $L$ and $D$—the target of diffusion experiments—are unknown at the outset of an experimental study. Repetition of experiments at specific conditions is the only reliable way to obtain Type B profiles.

### 4.2. Fast-path diffusion results

A detailed table of experimental results on oxygen diffusion, in titanite was presented in another paper (Zhang et al., 2006). In this study, two Arrhenius relations for fast-path diffusion were reported, one for experiments under dry conditions, the other for hydrothermal conditions:

$$D_{\mathrm{dry}} = 4.03 \times 10^{-2}(\mathrm{m^2/s})\exp(-313 \pm 22)\ (\mathrm{kJ/mol})/RT$$
$$D_{\mathrm{wet}} = 3.48 \times 10^{-7}(\mathrm{m^2/s})\exp(-219 \pm 39)\ (\mathrm{kJ/mol})/RT$$

From Fig. 7, it is clear that the fast-path diffusivity is 4–5 orders of magnitude higher than lattice diffusivities both under dry and wet conditions. As with lattice diffusion, the presence of water also reduces the activation energy for fast-path diffusion. A $T$-test of the fitted slopes of the two Arrhenius lines indicates that they are different statistically. Fig. 8 shows that in the 700–900 °C temperature range of the experiments, the differences between diffusivities for dry and wet conditions are not large. Diffusivities under hydrothermal conditions are slightly smaller than those under dry conditions, but if we extrapolate the data to lower temperature, wet diffusion will be faster than dry diffusion. At temperatures of geological interest, the difference is not significant.

### 4.3. Effect on bulk closure

Fast-path diffusion is coupled with lattice diffusion, and its overall effect on bulk diffusion will depend on the magnitude of the lattice diffusivity as well as the density of fast-paths. The contribution due to fast diffusion paths can be observed because the diffusants leave these paths and diffuse laterally into the crystal lattice through lattice diffusion. Hence, we cannot separate out independently the contribution due to fast-path diffusion. The volume of the fast-paths is generally very small compared to the volume of the crystal; consequently, the amount of diffusant present within these paths is usually very small, and therefore would make a negligible contribution to the amount of diffusant transported through the material.

In order to evaluate the effect of fast-path diffusion on the bulk closure properties of a crystal, we need to know

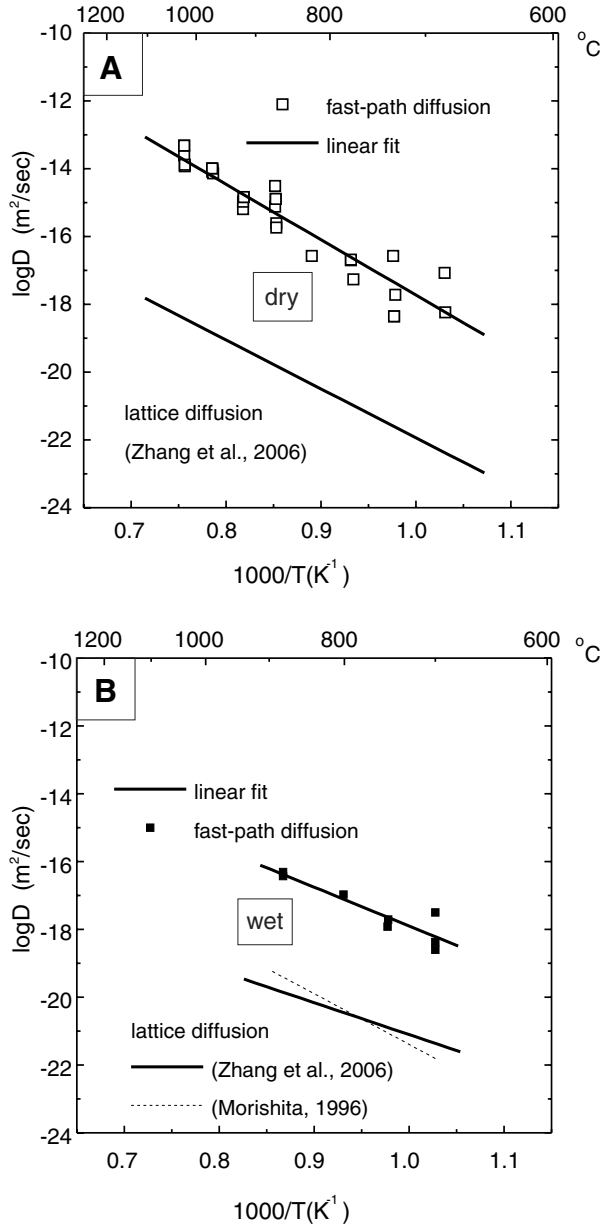


Fig. 7. Arrhenius plots for fast-path oxygen diffusion in titanites, under dry (A) and hydrothermal (B) conditions. The lattice diffusion data are also plotted for comparison. (A) From the fit to the dry fast-path diffusion data, an activation energy of $313 \pm 22$ kJ/mol and pre-exponential factor of $4.03 \times 10^{-2}$ m$^2$/s ($\log D_0 = -1.40 \pm 0.98$) are obtained. (B) From the hydrothermal fast-path diffusion data with water pressure at 100 MPa, we obtain an activation energy of $219 \pm 39$ kJ/mol and pre-exponential factor of $3.48 \times 10^{-7}$ m$^2$/s ($\log D_0 = -6.46 \pm 1.95$).

the three-dimensional distribution of these fast diffusion paths. The diffusion profile itself can not provide any insight because our experiments introduce diffusants only into a thin layer on the very surface of the crystal slab, and our profiling methods measure only a very thin layer of the crystal and commensurately short diffusion profiles. We already know that the fast-paths are not uniformly distributed within the crystal, since crystal slabs cut from same

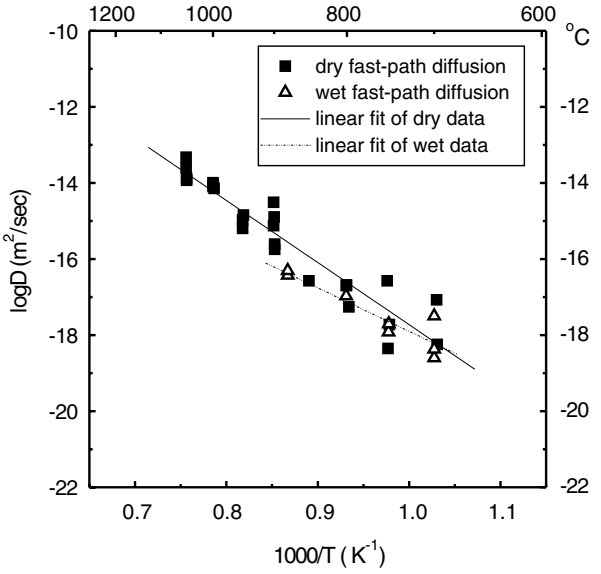


Fig. 8. Comparison of oxygen fast-path diffusion data in titanite between wet and dry conditions. Over the temperature range of the experiments, the differences between diffusivities for dry and wet conditions are not great.

crystal show varied behavior. The AFM images seem to indicate that the fast-paths are not interconnected over distances that are significant in proportion to the entire crystal. It thus seems likely that under most conditions fast-paths do not affect the oxygen bulk closure properties of titanite crystals because they do not provide a diffusive "shortcut" over long distances within the crystal.

## 5. CONCLUDING REMARKS

This study has shown that even when "perfect" crystals are difficult to obtain, crystals containing some extended defects can still be used to obtain reliable diffusivities as long as 'anomalous' diffusion profiles are recognized and an appropriate data reduction method implemented. The simple method we propose here for dealing with 'tailed' profiles is also suitable for diffusion in polycrystalline materials. The relative defect density concept is very useful as a guild for selecting experimental conditions for grain-boundary diffusion studies. Through this study we conclude that the fast-paths for oxygen diffusion in titanite are probably planar defects whose length is small relative to the crystal size. These defects are not uniformly distributed and do not appear to be inter-connected over long distances, so they are unlikely to significantly affect the bulk closure properties of titanite crystals.

## ACKNOWLEDGMENTS

We thank Jay Thomas for assistance with the atomic force microscopy. The manuscript benefited from perceptive and thorough reviews by Dr. Jim Van Orman. We also thank Dr. Mark Harrison for his editorial comments. This research was supported by NSF through the Grants EAR-0073752 and EAR-0440228 to Dr. E.B. Watson.

## REFERENCES


Amami B., Addou M., Millots F., Sabiono A., and Monty C. (1999) Self diffusion in $\alpha$-$Fe_2O_3$ natural single crystals. *Solid State Ionics* **5**, 358–370.

Cawley J. D., Lalloran J. W., and Cooper A. F. (1991) Oxygen tracer diffusion in single-crystal alumina. *J. Am. Ceram. Soc.* **74**, 2086–2092.

Cherniak D. J. (1990) A particle-accelerator based study of major and trace element diffusion in minerals. Ph.D. Thesis, State University of New York at Albany, Albany N.Y., 219 pp.

Farver J. R., and Yund R. A. (1991) Measurement of oxygen grain boundary diffusion in natural, fine-grained, quartz aggregates. *Geochim. Cosmochim. Acta* **55**, 1597–1607.

Farver J. R., and Yund R. A. (1995) Grain boundary diffusion of oxygen, potassium and calcium in natural and hot-pressed feldspar aggregates. *Contrib. Mineral. Petol.* **118**, 340–355.

Farver J. R., and Yund R. A. (1998) Oxygen grain boundary diffusion in natural and hot-pressed calcite aggregates. *Earth Planet. Sci. Lett.* **161**, 189–200.

Harrison L. G. (1961) Influence of dislocation on diffusion kinetics in solids with particular reference to alkali halides. *Trans. Faraday Soc.* **57**, 1191–1199.

Joesten R. (1991) Grain boundary diffusion kinetics in silicate and oxide minerals. In *Diffusion, atomic ordering, and mass transport-selected topics in geochemistry. Advances in Physical Geochemistry*, vol. 8 (ed. J. Ganguly). Springer-Verlag, pp. 345–395.

Kaur I., and Gust W. (1989) *Fundamentals of Grain and Interphase Boundary Diffusion*, Second Revised Edition. Ziegler Press, Stuttgart, 422 pp.

Le Claire A. D. (1963) The analysis of grain boundary diffusion measurements. *J. Appl. Phys.* **14**, 351–356.

Le Claire A. D., and Rabinovitch A. (1981) A mathematical analysis of diffusion in dislocations: I. Application to concentration "tail". *J. Phys. C: Solid State Phys.* **14**, 3863–3879.

Le Gall M., and Lesage B. (1994) Self-diffusion in $\alpha$-$Al_2O_3$ I. Aluminum diffusion in single crystals. *Philos. Mag. A* **70**, 761–773.

Levine H. S., and MacCallum C. J. (1960) Grain boundary and lattice diffusion in polycrystalline bodies. *J. Appl. Phys.* **31**, 595–599.

Mishin Y., and Herzig C. (1999) Grain boundary diffusion: recent progress and future research. *Mat. Sci. Eng. A* **260**, 55–71.

Moore D. K., Cherniak D. J., and Watson E. B. (1998) Oxygen diffusion in rutile from 750 to 1000 °C and 0.1 to 1000 MPa. *Am. Miner.* **83**, 700–711.

Prot D., and Monty C. (1996) Self-diffusion in $\alpha$-$Al_2O_3$ II. Oxygen diffusion in "undoped" single crystals. *Philos. Mag. A* **73**, 899–917.

Prot D., Le Gall M., Lesage B., Huntz A. M., and Monty C. (1996) Self-diffusion in $\alpha$-$Al_2O_3$ IV. Oxygen grain boundary self-diffusion in undoped and yttria-doped alumina polycrystals. *Philos. Mag. A* **73**, 935–949.

Reddy K. P. R., and Cooper A. R. (1982) Oxygen diffusion in sapphire. *J. Am. Ceram. Soc.* **65**, 634–638.

Van Orman J. A., Fei Y., Hauri E. H., and Wang J. (2003) Diffusion in MgO at high pressures: Constraints on deformation mechanisms and chemical transport at the core-mantle boundary. *Geophys. Res. Lett.* **30**. Art., No.1056.

Watson E. B., and Cherniak D. J. (1997) Oxygen diffusion in zircon. *Earth Planet. Sci. Lett.* **148**, 527–544.

Whipple R. T. P. (1954) Concentration contours in grain boundary diffusion. *Philos. Mag.* **45**, 1225–1236.

Yurimoto H., and Nagasawa H. (1989) The analysis of dislocation pipe radius for diffusion. *Mineral. J* **14**, 171–178.

Yurimoto H., Morioka M., and Nagasawa H. (1989) Diffusion in single crystals of melilite: I. Oxygen. *Geochim. Cosmochim. Acta* **53**, 2387–2394.

Yurimoto H., Morioka M., and Nagasawa H. (1992) Oxygen self-diffusion along high diffusivity paths in forsterite. *Geochem. J.* **26**, 181–188.

Zhang X. Y., Cherniak D. J., and Watson E. B. (2006) Oxygen diffusion in titanite: lattice diffusion and fast-path diffusion in single crystals. *Chem. Geol.* **235**, 105–123.


*Associate editor:* T. Mark Harrison